LIMNOLOGY and OCEANOGRAPHY

ASLO

Limnol. Oceanogr. 65, 2020, 455–470

doi: 10.1002/lno.11313

Testing the Canyon Hypothesis: Evaluating light and nutrient controls of phytoplankton growth in penguin foraging hotspots along the West Antarctic Peninsula

Filipa Carvalho [1,2*], **Jessica N. Fitzsimmons** [2,3], **Nicole Couto** [2,4], **Nicole Waite** [2], **Maxim Gorbunov** [2], **Josh Kohut** [2], **Matthew J. Oliver** [5], **Robert M. Sherrell** [2,6], **Oscar Schofield** [2]

[1]National Oceanography Centre, Southampton, UK
[2]Center for Ocean Observing Leadership, Department of Marine and Coastal Sciences, Rutgers University, New Brunswick, New Jersey
[3]Department of Oceanography, Texas A&M University, College Station, Texas
[4]Scripps Institution of Oceanography, University of California San Diego, La Jolla, California
[5]College of Earth, Ocean and Environment, University of Delaware, Lewes, Delaware
[6]Department of Earth and Planetary Sciences, Rutgers University, Piscataway, New Jersey

Abstract

Biological hotspots along the West Antarctic Peninsula (WAP) are characterized by high phytoplankton productivity and biomass as well as spatially focused penguin foraging activity. While unique physical concentrating processes were identified in one of these hotspots, understanding the mechanisms driving the blooms at these locations is of high importance. Factors posited to explain the blooms include the upwelling of macronutrient- and micronutrient-enriched modified Upper Circumpolar Deep Water (mUCDW) and the depth of the mixed layer influencing overall light availability for phytoplankton. Using shipboard trace-metal clean incubation experiments in three different coastal biological hotspots spanning a north-south gradient along the WAP, we tested the Canyon Hypothesis (upwelling) for enhanced phytoplankton growth. Diatoms dominated the Southern region, while the Northern region was characterized by a combination of diatoms and cryptophytes. There was ample concentration of macronutrients at the surface and no phytoplankton growth response was detected with the addition of nutrient-enriched mUCDW water or iron solution to surface waters. For all treatments, addition of mUCDW showed no enhancement in phytoplankton growth, suggesting that local upwelling of nutrient-enriched deep water in these hotspots was not the main driver of high phytoplankton biomass. Furthermore, the dynamics in the photoprotective pigments were consistent with the light levels used during these incubations showing that phytoplankton are able to photoacclimate rapidly to higher irradiances and that in situ cells are low light adapted. Light availability appears to be the critical variable for the development of hotspot phytoplankton blooms, which in turn supports the highly productive regional food web.

Coastal waters of the West Antarctic Peninsula (WAP) support a highly productive ecosystem and have been historically associated with large, diatom-dominated phytoplankton blooms (Nelson and Smith 1991; Prézelin et al. 2004; Smith et al. 2008). Additionally the WAP has several "biological hotspots" located at particular locations along the WAP continental shelf (Schofield et al. 2013) that are associated with the major penguin rookeries (Fraser and Trivelpiece 1996; Erdmann et al. 2011). Rapid changes in atmospheric and oceanic temperatures over the past six decades have had significant effects on the WAP ecosystem (Ducklow et al. 2012). Summer chlorophyll concentrations have declined about 12% over the past three decades (Montes-Hugo et al. 2009), accompanied with a shift in the community structure from larger diatoms to smaller celled ($< 20\ \mu m$) cryptophytes (Moline et al. 2004; Montes-Hugo et al. 2009).

Seasonal phytoplankton dynamics have been linked to the timing of sea ice retreat (Ducklow et al. 2012; Rozema et al. 2017; Schofield et al. 2017). Increased phytoplankton production is often observed in the spring along the retreating ice edge, where ample supply of nutrients at the surface

*Correspondence: filipa.carvalho@noc.ac.uk

Additional Supporting Information may be found in the online version of this article.

combined with increased water column stability and shallower mixed layer depth (MLD) provide favorable conditions for phytoplankton to grow. In the Northern WAP and as far south as Palmer Deep canyon (PD), reduced sea ice cover, increased winds and cloud formation have been accompanied by a deepening of the mixed layer (ML) and consequent reduction in the phytoplankton biomass (Montes-Hugo et al. 2009) through 2009. Sea ice previously lasted for longer periods for most of the Mid-WAP, where Marguerite Trough (MT) is located, and as the annual days of sea ice have decreased (Stammerjohn et al. 2008) there has been an increase in primary production (Montes-Hugo et al. 2009; Venables et al. 2013). Positive chlorophyll anomalies have been observed gradually throughout the years starting as early as 2009 in the Northern stations and later on in the most Southern stations evaluated (Kim et al. 2018), and is associated with increased sea ice since 2009/2010 (Schofield et al. 2018). This increase in sea ice has since reversed itself and is consistent with the long-term declines.

WAP biological "hotspots" (Schofield et al. 2013) are consistently found at cross-shelf submarine canyon systems, an observation which has led to the Canyon Hypothesis: primary production is enhanced at those locations as a result of water column dynamics, reduced sea ice coverage, and an ample reservoir of macro- and micronutrients (Kavanaugh et al. 2015) supplied by local upwelling. As in most parts of the Antarctic shelf, macronutrients are abundant along the WAP shelf (Serebrennikova and Fanning 2004; Ducklow et al. 2012; Kim et al. 2016), as deep winter mixing resupplies nutrients to the surface layers annually. Although macronutrients show marked seasonality (Clarke et al. 2008), they do not limit primary production (Holm-Hansen and Mitchell 1991) except during extreme phytoplankton blooms (Kim et al. 2016). Instead, any nutrient limitation on the WAP has been hypothesized to result from insufficient iron supply (Garibotti et al. 2005). Previous studies have speculated that intrusions of modified Upper Circumpolar Deep Water (mUCDW) onto the WAP shelf provide a source of the micronutrient iron that fuels primary production over the shelf (Prézelin et al. 2000, 2004), which, in turn, supports a productive regional food web (Schofield et al. 2010). This topographically forced flow of warm, micronutrient-enriched deep water interacts with bathymetry, promoting mixing across the shelf (Martinson et al. 2008; Martinson and McKee 2012; Couto et al. 2017; McKee et al. 2019) that could advect dissolved iron from deep sources to the upper water column.

Recent measurements of iron distributions on the shelf demonstrate, in fact, that iron concentrations in outer shelf and slope surface waters are much lower than on the inner shelf and near the canyon heads, and suggest that shelf sediment or glacial meltwater iron sources may be more important to coastal productivity than iron carried by off-shelf mUCDW. Additionally, a very recent and detailed study of dissolved iron (Fe) distributions around the vicinity of Palmer Deep indicates that the Fe supplying the regional euphotic zone comes from relatively shallow sediments surrounding the canyon, delivered by mixing in the upper 100 m, suggesting that glacial meltwater and upwelling of mUCDW are relatively unimportant Fe sources (Sherrell et al. 2018). This evidence counters the Canyon Hypothesis, that local canyon driven upwelling is required to supply this critical micronutrient to the surface layer (Sherrell et al. 2018). Accordingly, previous studies in coastal waters of the WAP have shown that inshore regions, including the three "biological hotspots" of the Canyon Hypothesis, do not show signs of Fe-limited primary production (Hopkinson et al. 2007; Annett et al. 2015; Carvalho et al. 2016).

Light is another major factor hypothesized to control primary production in the WAP shelf and other biological hotspots along the Antarctic coast. Both the MLD and water column stability have been widely linked to phytoplankton dynamics (Holm-Hansen and Mitchell 1991; Sakshaug et al. 1991; Moline and Prezelin 1996; Carvalho et al. 2016). Phytoplankton live in a dynamic light environment that is controlled by a combination of incident light, MLD, and the rate of turbulent mixing (Lewis et al. 1984; Cullen and Lewis 1988). Since these fluctuations in the light environment vary over a wide range of timescales from seconds to hours, phytoplankton use a suite of physiological adaptations that have response times spanning these timescales. Under high light, phytoplankton take advantage of the xanthophyll cycle, a mechanism of nonradiative energy dissipation that prevents photooxidative damage to the photosynthetic apparatus (Falkowski and Raven 2007). In diatoms and dinoflagellates, the carotenoids responsible for this photoprotection are diatoxanthin (DT) and diadinoxanthin (DD) (Demers et al. 1991). High light induces the conversion of DD into its epoxy-free form, DT. Hence, the cellular abundances of DT and DD provide an indication of the light history, as exposure to high light promotes synthesis of these photoprotective pigments (Brunet et al. 1993). On shorter timescales (seconds to minutes), the only relevant process is the conversion of DD to DT, as there is no time for new pigment production to occur, and therefore DD + DT remains constant. Thus, the photoprotective pigment concentration (DT + DD) normalized to chlorophyll *a* (Chl *a*), (DT + DD)/T_{chl} is helpful in evaluating phytoplankton light history on timescales of days (Fujiki et al. 2003), while the ratio DT/(DD + DT) is a good indicator for light exposure on shorter timescales.

The relatively short food web in Antarctic ecosystems results in a higher vulnerability and dependency of the higher trophic levels on phytoplankton biomass under the krill grazing pressure (Bernard et al. 2012; Saba et al. 2014). Understanding the links between physical forcing and the consequent biological responses are therefore of high importance. Here, we present results from shipboard incubation experiments conducted to evaluate whether light or nutrients underlie the phytoplankton blooms at three previously identified biological hotspots in the WAP (Schofield et al. 2013). A recent study used high frequency radar data and a series of particle release experiments to estimate surface residence times across PD (Kohut et al. 2018).

Their findings suggest that these biological hotspots do not necessarily reflect phytoplankton growth in situ, but instead act as phytoplankton concentrating mechanisms, as calculated residence times of surface waters are shorter than phytoplankton growth rates. This would imply that the biological "hotspots" are not actually sites of extreme phytoplankton blooms in response to local forcings but instead reflect a concentrated amalgamation of biomass from several typical nearshore spring blooms. The authors also found regional differences across the canyon where increased residence times in the Northern region explain the increased chlorophyll concentration found by Carvalho et al. (2016), showing that, given time, phytoplankton do grow locally.

Given these recent and somewhat divergent findings, the current study does not intend to explain why these canyons are biological hotspots. Instead, we test which of two potential mechanisms, given sufficient time, would control phytoplankton composition and production in these biological hotspots: (1) the regular upwelling of mUCDW near the coast triggers a phytoplankton bloom through the supply of both macro- and micronutrients to the surface waters and/or (2) the spring phytoplankton bloom is initiated by light, where the shallowing of the MLD relieves the phytoplankton community of light limitation. We show that phytoplankton in these coastal canyon systems are nutrient-replete throughout the growing season, and thus light is a better modulator of in situ blooms in these regions. Furthermore, this study verifies that phytoplankton in these canyons show efficient use of photoacclimation mechanisms to high light that allows them to thrive under variable environmental conditions.

Materials and methods

Experimental approach and water collection

Shipboard incubation experiments were conducted at three biological hotspots (Fig. 1a) during the annual Palmer Long-Term Ecological Research (PAL-LTER) cruise in January 2015 along the WAP, onboard the ARSV *Laurence M. Gould* (cruise LMG15-01). These biological hotspots have been identified by the presence of major breeding colonies for the Adélie penguins in the WAP (Schofield et al. 2013). Additionally, increased phytoplankton biomass in these regions was evident from satellite observations of ocean color (Kavanaugh et al. 2015) where phytoplankton biomass increases were found between November and March, with peak biomass found in January (Kavanaugh et al. 2015; Kim et al. 2018). The Northernmost site was located at PD near Anvers Island (64.91°S, 64.58°W); a Mid-WAP site was located at MT near Avian Island (68.03°S, 69.28°W); and the third site was at the Southernmost accessible point along the ice edge off of Charcot Island (CI) (69.11°S, 76.45°W).

Source waters for incubation experiments (Table 1) were collected using a trace metal-clean (TMC) rosette (Sherrell et al. 2018). A Conductivity-Temperature-Depth (CTD) sensor package mounted on the frame was used to obtain physical measurements down the water column (Fig. 1b–d; *see* "Macro- and micronutrient analysis" section for details). Acid-washed, clear polycarbonate 1-liter incubation bottles were filled with source waters in the volume ratios described below. Water used in the incubations was prefiltered using an acid-washed polyester mesh to remove macrozooplankton over 350 μm.

Two sets of shipboard incubation experiments were conducted at each location to evaluate separately the importance of light (reflecting variable MLDs) and the upwelling of nutrient-enriched mUCDW (nutrient addition experiments) in controlling phytoplankton blooms over submarine canyons in the WAP. "Deep" water was collected at the depth of temperature maximum (T_{max}) which is one of the signatures of mUCDW on the shelf; "surface" water was collected from 10 to 15 m depth and in the upstream direction of the dominant current flow to prevent contamination from the ship.

In both experiments, variables were measured at setup (T_i), and then the full incubation bottle was sacrificed after 4 d of incubation (T_f). Similar incubation experiments conducted along the WAP prior to this study, with sampling time points at 0, 1, 2, 4, and 7 d, show that the phytoplankton take at least 4 d before showing exponential growth (F. Carvalho unpubl. data). The incubation duration was chosen to compromise between the requirement to observe a significant response (i.e., an increase in biomass), yet to minimize the artifacts of the bottle effects. Because the rates of metabolic reactions in the cell are reduced under low temperature, shorter-term incubations (~ 1 d) are not sufficient; instead, 3–4 d are typical durations used in the Antarctic waters (Coale et al. 2004; de Baar et al. 2005). Measurements at both time points included Chl *a* and accessory pigments for community composition classification, nutrient concentrations, and photosynthetic efficiency using variable fluorescence techniques (Gorbunov and Falkowski 2004).

Physical measurements

MLDs were calculated from the vertical profiles of temperature and salinity using the method described in Carvalho et al. (2017). A quality index (QI) was also determined to quantify the uncertainty of the MLD computation, where 0.5 sets the threshold between MLD not determined (< 0.5) or determined (> 0.5), respectively. This approach was validated recently using ship-based study in the WAP (Schofield et al. 2018). In order to assess the photoacclimation status of phytoplankton and to estimate the effective in situ photosynthetically available radiation (PAR) exposures, changes in light intensity due to cloud cover were analyzed using a mast-mounted PAR sensor (Fig. 2).

As the TMC rosette did not have a PAR sensor and sampling occurred independently of the hour of the day (24-h CTD operations), the depth for the 1% light level (i.e., euphotic zone) was calculated by reconstructing the vertical profiles of PAR

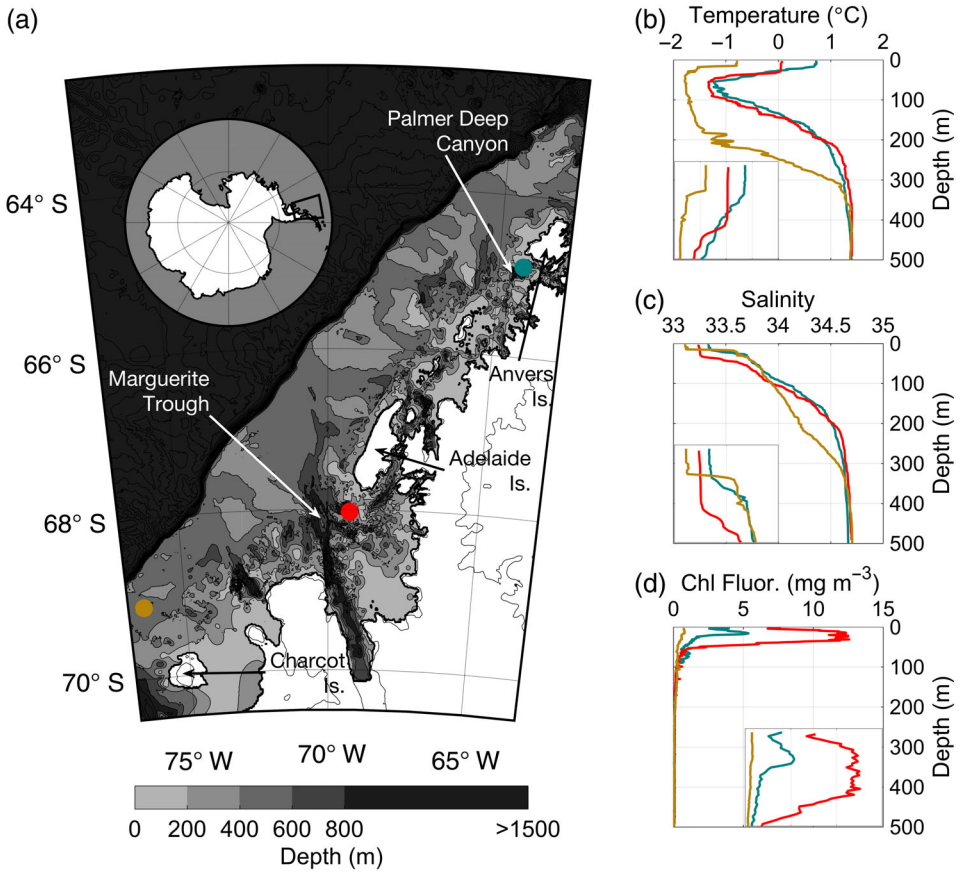

Fig. 1. (**a**) Bathymetry maps with the locations of the water collection sites for the incubation experiments conducted along submarine canyons in the WAP: PD (teal), MT (red), and canyon near CI (gold). Depth profiles of (**b**) temperature, (**c**) salinity, and (**d**) chlorophyll fluorescence from CTD casts of source waters at the three incubation sites. The inset gray boxes on the right panels show the upper 50 m on an expanded depth scale for clarity. Colors denote cast location.

Table 1. Relevant initial variables from the incubation water collection casts for all three sites (PD, MT, region near CI), including water source, depth of sampling for incubation setup, Chl *a* concentration, and initial F_v/F_m. For each cast, we report macronutrients and dissolved (< 0.2 μm) Fe concentrations, MLD, and corresponding QI (following Carvalho et al. 2017) as well as 1% light level at the euphotic zone water collection depth.

Site	MLD (m) (QI)	1% light level (m)	Water source	Depth (m)	Chl *a* (μg L^{-1})	F_v/F_m	[N + N] (μmol L^{-1})	[PO_4] (μmol L^{-1})	[SiO_4] (μmol L^{-1})	[Fe] (nmol L^{-1})
PD	26 (0.52)	19.8	Surface	10	4.24	0.40	20.68	1.57	60.37	0.49
			Deep	1200	0	—	27.13	1.96	73.11	1.49
MT	44 (0.56)	15.8	Surface	10	12.9	0.39	8.34	0.70	40.66	0.18
			Deep	490	0	—	29.02	2.06	76.86	0.61
CI	15 (0.89)	47.5	Surface	15	0.67	0.31	23.11	1.64	48.50	0.12
			Deep	440	0	—	27.25	1.97	67.08	0.31

(Fig. 3) from chlorophyll profiles, using HydroLight (Mobley 1994). Default HydroLight settings were used for these simulations. These modeled PAR profiles were then used to evaluate the phytoplankton light history (Fig. 2) by averaging PAR over the ML from the 2 d prior to collection casts (MLD_{ave} PAR, Table 2).

Micronutrient experiments

In the first set of experiments, we tested the "Canyon Hypothesis" by evaluating whether the upwelling of warm, nutrient-enriched mUCDW enhanced phytoplankton photosynthetic efficiency and growth at these biological hotspots. Two different treatments were set: one surface (S) with

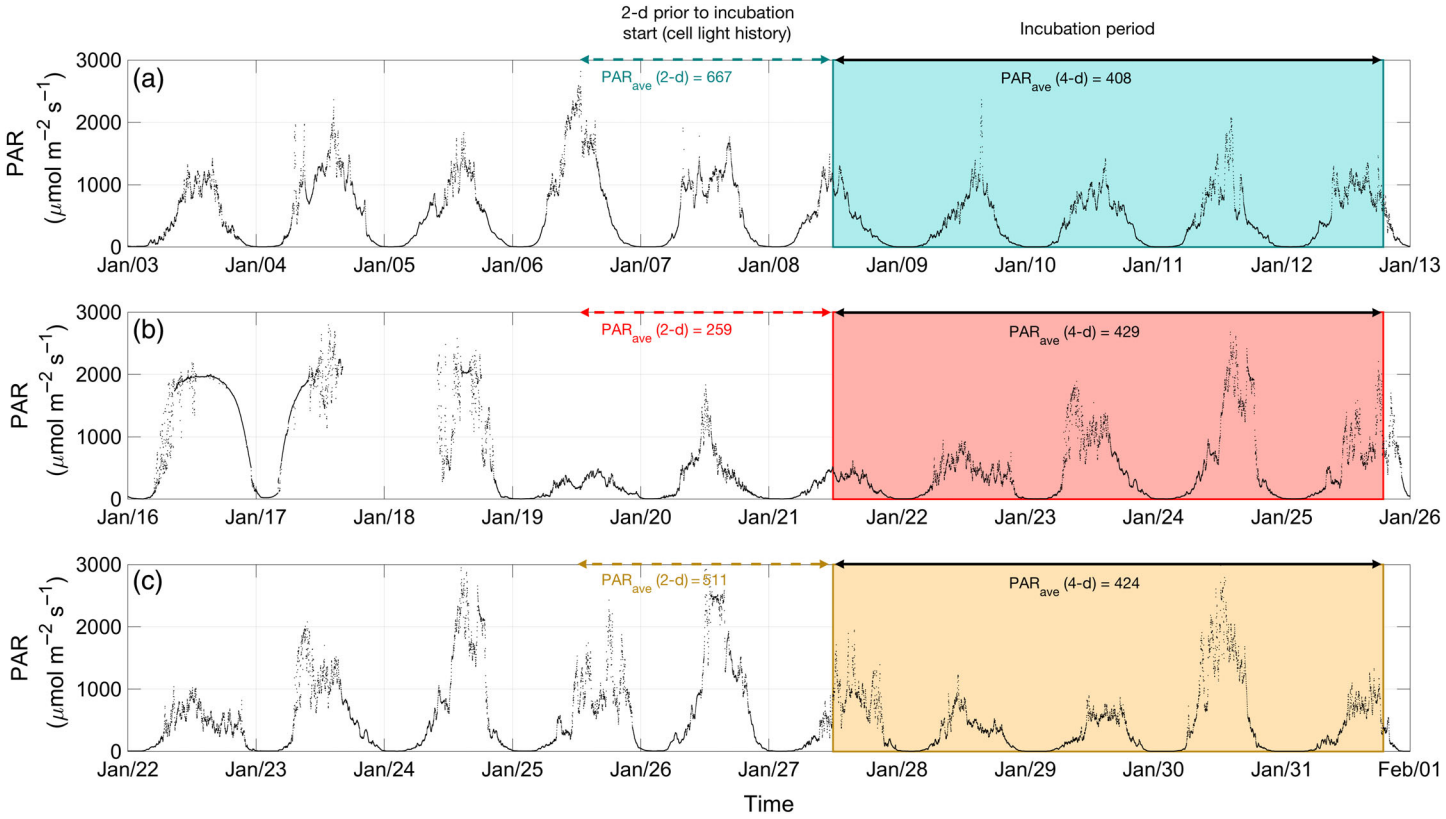

Fig. 2. Surface PAR (μmol m^{-2} s^{-1}) for the period preceding and during each experiment: (**a**) PD, (**b**) MT, and (**c**) region near CI. Incubation periods indicated by the colored box. Also reported are the Average incident PAR for the 2-d period prior to water collection (dashed colored arrow) which sets the phytoplankton light history and the 4-d average incident PAR (solid black arrow) which is used to calculate the light levels at each light treatment during incubation (Table 2).

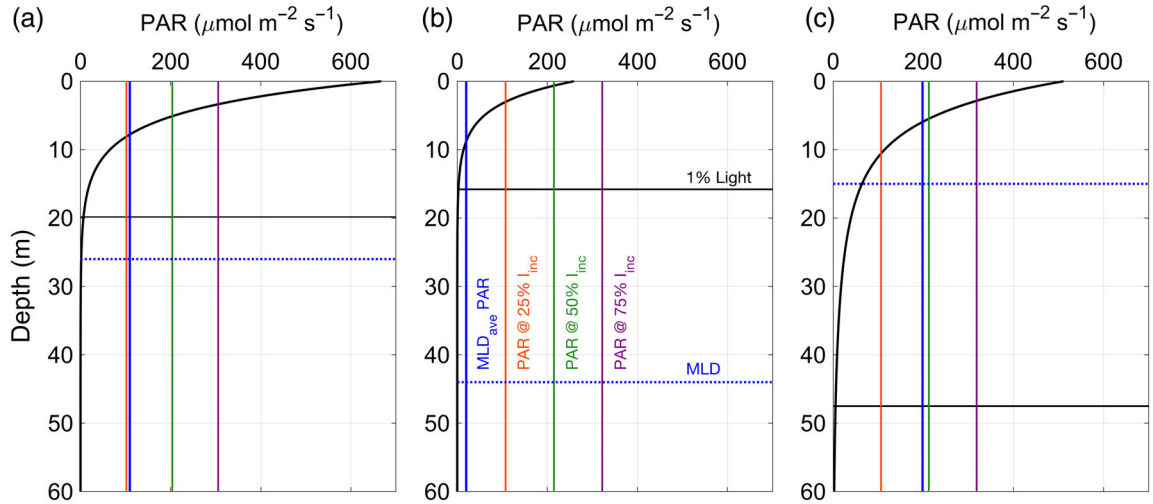

Fig. 3. Photosynthetically available radiation (black line) profiles from collection casts for all three regions modeled using HydroLight: (**a**) PD, (**b**) MT, and (**c**) region near CI. Vertical lines indicate average light level when screened to 75% (purple), 50% (green), and 25% (orange) of the incident radiation during the incubation experiment, where incident radiation is the average surface PAR during the 4-d incubation. Blue dotted and black solid horizontal lines indicate MLD and 1% light level for each region, respectively. The blue vertical line represents the average PAR within the ML (from Table 2).

"surface" water only, and one mix (M) where equal volumes of "surface" and "deep" water were mixed, totaling equivalent 1.0 L volumes in each treatment. Given that no phytoplankton were present in the "deep" water, half of the "surface" water in the S treatments was filtered through an acid-cleaned, 0.2 μm filter (Acropak-200, Pall) inside of a self-fabricated

Table 2. Average incident PAR (μmol m^{-2} s^{-1}) for the 2-d period prior to incubation start and for the 4-d incubation duration for all two sites (PD, MT, region near CI). Modeled MLD averaged PAR (MLD_{ave},) indicates phytoplankton light acclimation history. Average light for each screening used (75%, 50%, and 25%) is also shown, considering the 4-d average incident PAR during incubation.

	2-d average prior to incubation		4-d average during incubation			
Site	Incident PAR (PAR_{inc})	MLD_{ave}	Incident PAR (PAR_{inc})	75% PAR_{inc}	50% PAR_{inc}	25% PAR_{inc}
PD	667	109	408	305	204	102
MT	259	20	429	322	215	107
CI	511	198	424	318	212	106

clean room bubble (Annett et al. 2017) so that all treatments started with the same phytoplankton biomass. For each treatment, three replicates were spiked with 100 μL of a solution of 17.9 μmol L^{-1} Fe^{3+} made from an $FeCl_3$ stock standard diluted into 0.24 mol L^{-1} ultrapure hydrochloric acid to give a final Fe addition of 1.8 nmol L^{-1} ("+" treatments, with no significant effects on solution pH), and three bottles were left unaltered as controls. Bottles were sealed and transferred to a seawater flow-through incubator shaded with a screen to provide an irradiance of ~ 50% of the incident sea surface irradiance inside the incubator. At T_f, incubation solutions were filtered through 0.2 μm membranes (Supor, 47 mm, Pall) for nutrient concentration analyses before any other measurements were made, to limit contamination. Analyses at setup of separate seawater samples from the same Niskin-X bottles for other micronutrient metals support our assumption that no other trace metal micronutrient has the potential to limit productivity (R. M. Sherrell unpubl. data).

Light experiments

The importance of light was evaluated by incubating bottles at different light levels, with an attempt to simulate different ML light regimes. Using the same mix treatment setup as in the above iron addition experiments (equal amounts of "surface" and "deep" water), each light treatment was incubated at 75%, 50%, and 25% of the incident sea surface irradiance. To prevent any potential iron limitation, the same Fe addition described in "Micronutrient experiments" section was added to all light treatments. Each treatment had three replicate incubation bottles.

High-performance liquid chromatography pigment analysis

Concentrations of Chl *a* and accessory pigments of phytoplankton were measured by high-performance liquid chromatography (HPLC), following the methods described by Wright (1991). At the end of each set of incubations, bottles were removed from the incubator and placed inside a blacked-out box, which was then closed to minimize the exposure to light and therefore preserve the pigments resulting from each treatment exposure. Bottles were then carried to the lab and filtration was done under dim light. Samples were filtered onto 25 mm GF/F filters, flash-frozen in liquid nitrogen, and stored at −80°C for postcruise pigment analysis.

Extraction was done using 98% methanol and 2% aqueous ammonium acetate and ultrasonicated while held on ice water (to keep cold) for 30 s. Samples were stored at −20°C for at least 2 h, then ultrasonicated again for 10 s, and centrifuged to separate filter from extract. Extract was put into vials and run on HPLC system. Pigments were separated using an Agilent 1100/1200 series system with a Diode Array Detector (Model G1315C, scanning wavelengths 275–800 nm) with a Zorbax Eclipse Plus C18 column, 4.6 × 250 mm, 5 μm. HPLC Grade phase eluents were used: Solvent A (80% methanol, 20% aqueous ammonium acetate, pH 7.2); Solvent B (90% acetonitrile, 10% water); and Solvent C (100% ethyl acetate). Peaks were quantified at 440 nm and pigment identification was based on retention time and spectral shape. Samples were manually checked for correct peak area and pigment identification. Any mistakes by the auto-identification of the Agilent software were corrected manually. Standard chlorophyll samples with known concentration (from a spectrophotometer reading) are run on the HPLC system daily to verify retention times and column calibration.

The concentrations of Chl *a* epimers and allomers, monovinyl Chl *a*, divinyl Chl *a*, chlorophyllide *a* were summed up and referred to as total Chl *a* (denoted from now on as T_{Chl}). Accessory pigments quantified by HPLC analysis included chlorophyll *b* (Chl *b*); chlorophyll c_1, chlorophyll c_2, and chlorophyll c_3; prasinoxanthin, fucoxanthin, 19′-hexanoyloxyfucoxanthin, 19′-butanoyloxyfucoxanthin, peridinin, DD, DT, alloxanthin, zeaxanthin, β-carotene, and α-carotene.

Phytoplankton community analysis

The taxonomic composition of the phytoplankton assemblages was derived from HPLC pigment data analysis with CHEMTAX V1.95 (Mackey et al. 1996), using initial pigment ratios previously derived from WAP phytoplankton (Kozlowski et al. 2011). In that study, the authors used 12 yr of pigment data in the WAP to derive a method to estimate the main phytoplankton taxa in the study region and included microscopy analyses for verification. Pigments used to derive community composition were chlorophyll c_2, Chl *b*, Chl *a*, fucoxanthin, alloxanthin, 19′-hexanoyloxyfucoxanthin, and 19′-butanoyloxyfucoxanthin. Output phytoplankton groups included diatoms, cryptophytes, prasinophytes, haptophytes,

and "mixed flagellates." While the first four groups have distinctive marker pigments, the latter one represents a range of taxa that includes both dinoflagellates and unidentified phytoflagellates. No photoacclimation state was taken into account (data were run in the same bin) as no significant differences were found in the final CHEMTAX ratios between different light bins (Kozlowski et al. 2011). While we were not able to collect microscopy samples for these experiments to fully validate our results, historical CHEMTAX data in this region have been validated using this same method (Kozlowski et al. 2011).

Macro- and micronutrient analysis

Water samples from all experiments were collected at T_i and T_f for macronutrient determination of nitrate + nitrite (N + N), phosphate (PO_4^{3-}), and silicate (H_4SiO_4). Samples were filtered through GF/F filters and stored frozen at −20°C in 15 mL acid-rinsed Falcon™ centrifuge tubes until analysis at Lamont Doherty Earth Observatory (Columbia University, NY) using a SEAL Analytical AutoAnalyzer AA3 HR, Software version 6.10 (Mequon, WI), G-297-03 Rev 4 (Multitest MT19 for PO_4^{3-}), G-172-96 Rev 16 (Multitest MT 19 for NO_3^- and NO_2^-), and G-177-96 Rev 11 (Multitest MT19 for H_4SiO_4). Standards used for the phosphate, nitrate + nitrite, and silicate analyses were potassium dihydrogen phosphate, potassium nitrate and sodium nitrite, and sodium metasilicate nonahydrate, respectively. The Joint Global Ocean Flux Study (JGOFS) Methods (1994) were used for all macronutrient analyses.

Trace metal methods

Seawater samples for iron analysis were collected using the TMC rosette composed of 12 Teflon-coated Niskin-X bottles mounted on a polyurethane-coated aluminum frame that was free of metal anodes and included epoxy encased lead weights (Annett et al. 2017; Sherrell et al. 2018). The rosette was deployed using a plastic-coated aramid conducting cable through an anodized aluminum sheave. The Niskin-X bottles were stored and prepped in a metal-free "bubble" composed of plastic sheeting over a wooden frame and inflated using High-efficiency particulate air (HEPA)-filtered air to avoid metal contamination from laboratory air. Immediately before each cast, each bottle was carried individually from the bubble and mounted on the rosette, and bottles were opened on deck for as short a time as possible to minimize deck contamination. Bottles were tripped on ascent at < 10 m min^{-1} to ensure that the seawater sample was collected as the rosette moved into seawater uncontaminated by any of the CTD components mounted on the lower frame. Filled Niskin bottles were returned to the trace metal bubble as soon as possible after recovery in order to prevent deck contamination.

Once in the bubble, each Niskin-X bottle was pressurized to ~ 4 psi using an air manifold fed by HEPA-filtered compressed air. An acid-cleaned piece of Bev-A-Line tubing was secured in the stopcock and rinsed with sample seawater before an acid-cleaned Acropak-200 (0.2 μm) capsule filter was added onto the line. After the filter was flushed with ~ 1 L of seawater, acid-cleaned Low-density polyethylene (LDPE) bottles were filled with filtered seawater following three ~ 10%-volume bottle rinses. Samples were acidified to pH 2 with concentrated hydrochloric acid (Optima grade, Fisher Scientific) for storage.

More than a year after acidification, filtered seawater samples were analyzed to determine Fe concentration using a modification of the isotope dilution-inductively coupled plasma mass spectrometry (ICP-MS) method of Lagerström et al. (2013). In short, samples were weighed into 30 mL LDPE bottles and spiked with a mixed isotope solution containing a known concentration of ^{57}Fe. Spiked seawater samples were automatically extracted using the commercially available SeaFAST pico system (Elemental Scientific) after online buffering to pH ~ 6.5 using ammonium acetate and a 25-fold preconcentration into 10% v/v nitric acid (Optima grade, Fisher Scientific). Within a few days, these samples were analyzed for ^{56}Fe and ^{57}Fe on an Element 1 (Finnigan MAT) high-resolution ICP-MS, in medium resolution. Analysis of SAFe standard seawater solutions was found to be within error of consensus values, indicating the high accuracy of this analytical method. Precision as determined by replicated analysis of a single sample is ± 3%.

In vivo chlorophyll and variable fluorescence

Photosynthetic efficiency of Photosystem II (F_v/F_m, or $[F_m - F_o]/F_m$) was measured using a Satlantic Fluorescence Induction and Relaxation (FIRe) system as described in (Gorbunov and Falkowski 2004), where F_o an F_m are minimum and maximum yields of chlorophyll fluorescence and F_v is variable fluorescence. All samples were kept under dim light conditions (ca. 5 μmol quanta m^{-2} s^{-1}) at in situ temperatures for > 30 min to alleviate the effects of nonphotochemical quenching and photoinhibition (Park et al. 2017). Fluorescence response was analyzed using FPRO Software developed by M. Gorbunov. For all samples, a 0.45-μm filtered sample was used to deduce the blank that was subsequently subtracted from the fluorescence signals (F_o and F_m). We quantified the response to nutrient enrichment or irradiance exposure by calculating the change in measured parameters relative to control at the final incubation time (T_f):

$$\Delta F_v/F_m(\%) = \left[(F_v/F_m)_{\text{treatment}} - (F_v/F_m)_{\text{control}}\right] / (F_v/F_m)_{\text{control}} \times 100, \quad (1a)$$

$$\Delta\sigma_{PSII}(\%) = \left[(\sigma_{PSII})_{\text{treatment}} - (\sigma_{PSII})_{\text{control}}\right] / (\sigma_{PSII})_{\text{control}} \times 100, \quad (1b)$$

where σ_{PSII} is functional absorption cross-section of PSII and the $(\,)_{\text{control}}$ is the mean of all three replicates for the control treatment.

To assess phytoplankton stress response between treatments, data reported in Fig. 7 show photosynthetic efficiency

(F_v/F_m) at the final timepoint normalized by the control treatment also at T_f, indicating the relative change in F_v/F_m between treatments and not timepoints. For the nutrient addition experiments, the controls were the no iron addition treatments, and for the light experiments, data are shown relative to the lowest irradiance treatment, 25%. Relative changes between timepoints for each treatment can be found in Table 3.

Statistical analyses

ANOVA was used to evaluate whether the mean values of total chlorophyll, photosynthetic efficiency, and photoprotective pigment ratios changed with time and treatments. A post hoc Tukey's honest significance test (Tukey test) was used to assess which treatment means were significantly different from each other.

Results

A total of six incubation experiments were conducted during the cruise, with one light experiment and one nutrient enrichment experiment at each sampling location (PD, MT, CI).

Palmer Deep canyon

PD, the northernmost site tested, showed a clear dissimilarity to the other two sites in terms of the light history (Fig. 2), phytoplankton community composition (Fig. 4), and the responses to the different incubation treatments (Figs. 5–7). Initial phytoplankton community structure at PD, evaluated by CHEMTAX analysis (Fig. 4), showed a mixed community composed mostly of diatoms and cryptophytes (~ 40% and 50%, respectively). Neither of the two other incubation sites had significant cryptophyte populations, making them unique to Palmer Deep. Then, with each nutrient or light treatment, it was the cryptophytes that increased in abundance between T_i and T_f, indicating that they were most responsive to the experimental variables.

For each incubation experiment, phytoplankton source waters were diluted in equal amounts of filtered seawater. At PD, surface water was collected with an initial phytoplankton biomass of 4.24 μg Chl a L^{-1} and mixed with filtered seawater, resulting in an initial concentration of 2.12 μg Chl a L^{-1} in the incubation bottle. Though cryptophytes increased in abundance in each treatment, overall biomass measured by total Chl a (T_{chl}) decreased significantly ($p < 0.001$) in all light treatments (Fig. 5). Given variable intracellular concentrations of total chlorophyll, observed chlorophyll decreases at PD can be partially due to the change in community composition from large diatoms to smaller-celled cryptophytes since the biomass gradient is controlled by cell size (Garibotti et al. 2003*b*). Since decreases in T_{chl} were only recorded at PD where small phytoplankton were abundant, it is likely that the relative increase in cryptophytes was the major reason for the observed decrease in T_{chl}.

Decreases in T_{chl} were accompanied by concomitant increases in photoprotective pigments (Fig. 6), as evident by the ratios (DT + DD)/T_{chl} and DT/(DD + DT). This shift in photoacclimation status was also evident from a characteristic decrease in σ_{PSII} derived from independent fluorescence measurements (Table 3). The lowest light level tested (25%) yielded significantly lower T_{chl} ($p < 0.001$) than the other two light treatments, with a significant change in community composition that promoted growth of mixed flagellates instead of cryptophytes (Fig. 4). This shift in dominant phytoplankton community under low irradiances is consistent with results from Schofield et al. (2017), where mixed flagellates were associated with deeper MLD (lower light). The magnitude of photoprotective carotenoid normalized to chlorophyll ratio (Fig. 6) is indicative of the degree of adaptation to low light, with phytoplankton at MT showing a ratio up to five times higher than at PD, indicating acclimation to lower light conditions at PD compared to MT.

Source waters in the ML showed replete concentrations of macronutrients and dissolved iron (Table 1). Although differences were found between initial and final timepoints, namely reduction in T_{chl} and a greater dominance of cryptophytes in terms of community composition, when comparing all the final timepoints of the nutrient treatments in this region, the addition of deep, nutrient-enriched mUCDW (M treatment) and iron additions ("+" treatments) resulted in no significant ($p > 0.05$) changes in T_{chl} (Fig. 5) and in community composition (Fig. 4).

Changes in photosynthetic efficiency of Photosystem II (F_v/F_m) at the final timepoint are reported in percentage and normalized to their respective control treatment. No significant changes in F_v/F_m ($p < 0.05$) were observed in the enrichment treatment (+) relative to its correspondent unenriched control. When comparing F_v/F_m between initial and final timepoints, significant changes were observed in all light

Table 3. Physiological parameters collected during the light incubation experiments for the three canyon systems (PD, MT, region near CI). Photosynthetic efficiency of Photosystem II or photosynthetic health (F_v/F_m) is presented for the starting population (T_i). Changes in F_v/F_m and the functional absorption cross-section of PSII ($\Delta\sigma_{PSII}$) are reported in percentage as the difference between T_i and T_f (final timepoint after 4 d), normalized by T_i.

		75% light		50% light		25% light	
Site	F_v/F_m at T_i	$\Delta F_v/F_m$	$\Delta\sigma_{PSII}$	$\Delta F_v/F_m$	$\Delta\sigma_{PSII}$	$\Delta F_v/F_m$	$\Delta\sigma_{PSII}$
PD	0.40	−65%	−7%	−62%	−28%	−28%	−34%
MT	0.39	−59%	−20%	−35%	−31%	−16%	−30%
CI	0.31	+22%	+25%	+32%	−8%	+64%	−8%

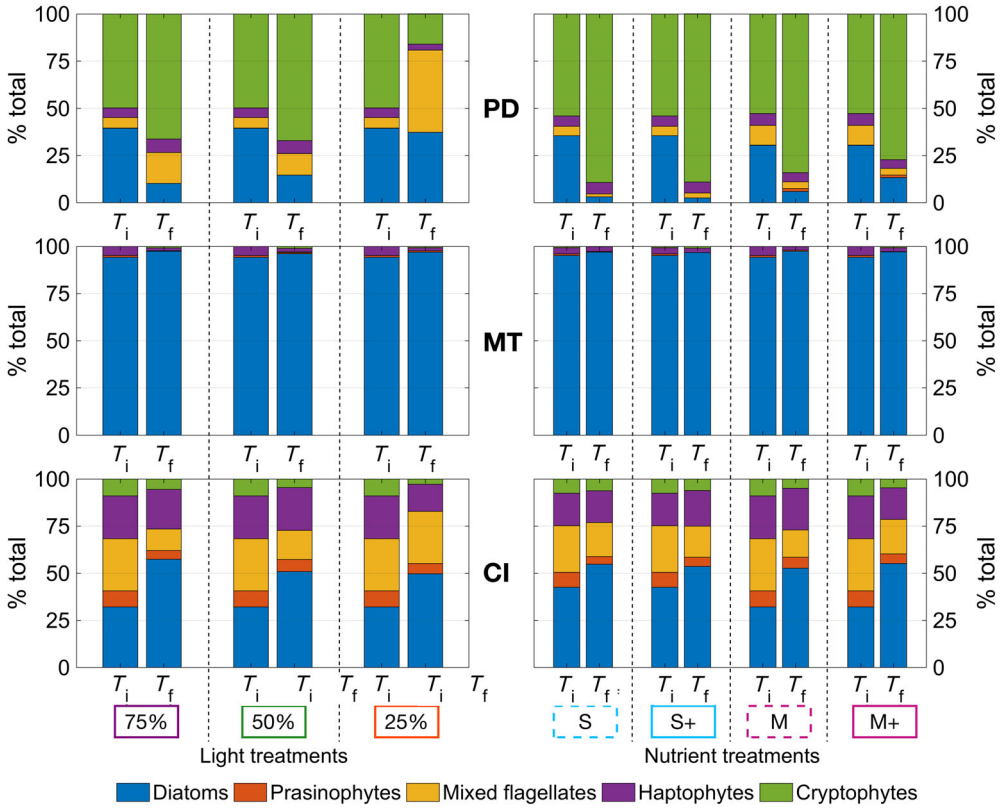

Fig. 4. Community composition results from CHEMTAX for the light (left) and nutrient (right) manipulation experiments at PD (top), MT (middle), and the canyon near CI (bottom). Light treatments are shown as the percentage of light screened from surface irradiance (75%, 50%, and 25%). Nutrient controls are shown as surface water only (S) and mix (M) treatment where surface water is mixed with equal amount of mUCDW with the corresponding iron addition treatments (S+ and M+). Main groups found are shown in color as diatoms, prasinophytes, mixed flagellates, haptophytes, and cryptophytes.

treatments, with declines recorded between 0.1 (−28%) and 0.25 (−65%) for irradiances 25% and 75%, respectively (Table 3). At the end of the incubation, when comparing F_v/F_m between light treatments relative to the lowest irradiance (25%), both higher irradiances resulted in a marked and significant decrease, affecting photosynthetic efficiency around 50% (± 18%). These incubations suggest that phytoplankton at PD had replete nutrients and that light was a major factor regulating the physiology and growth of the community. The incubations strongly suggest that cells were acclimated to low light (lower than the 25% incubation treatment) and any increase elicited a rapid light acclimation response.

Marguerite Trough

MT showed the highest phytoplankton biomass of the sites in the study. In contrast to PD, diatoms were the dominant phytoplankton group at this site (~ 95%) and there was no significant presence of cryptophytes. The light history of the populations in MT (Table 2) revealed that the light levels in the 2 d prior to the start of the incubation were at most half (average 259 μmol m^{-2} s^{-1}) those at PD and CI, mostly due to increased cloud cover (Fig. 3). Using the MLD during the water collection cast and the average incident radiation from the previous 2 d, we established the light history of the incubated phytoplankton cells by calculating the average PAR for the ML during the 2 d prior to collection (MLD$_{ave}$ PAR = 20 μmol m^{-2} s^{-1}, Table 2). With MLD (44 m) deeper than the euphotic depth (15.8 m) (Fig. 3b; Table 1), the diatom population at this site was low light adapted. Except for the highest irradiance tested (75%), growth was significant over the course of the incubation experiment as observed by increases in T_{chl} (Fig. 5, $p < 0.001$), suggesting phytoplankton were able to acclimate rapidly to higher irradiances. When exposed to a significantly higher light level during the 4-d incubation experiments (the average surface irradiance was 429 μmol m^{-2} s^{-1}), photoprotective pigment concentration normalized to chlorophyll showed the highest ratio among the three regions (Fig. 6).

Waters at MT are exposed to stronger winds than neighboring Ryder Bay, where many prior studies have reported shallower MLDs (Venables et al. 2013), possibly explaining the deep MLD recorded in MT. However, sustained 30-knot winds over the 24 h prior to water collection could have deepened the MLD and influenced our light history analysis by inferring an adaptation to much lower light than was in fact available to the population the preceding 48 h. Assessment of photosynthetic health (F_v/F_m) by variable fluorescence (Fig. 7) indicated, as at PD, a significant reduction at all incubation

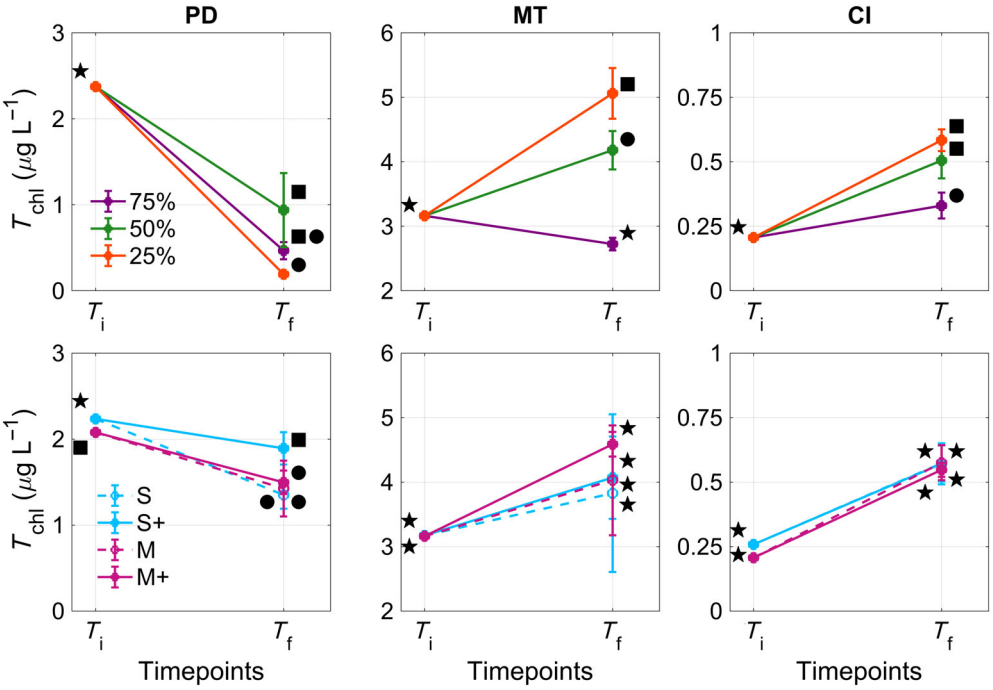

Fig. 5. Total Chl *a* (T_{chl}) at initial setup (T_i) and after 4 d (T_f) for PD (left), MT (middle), and canyon near CI (right). Light treatments are shown as percentage of surface irradiance (75%, 50%, and 25%). Nutrient controls are shown as surface (S) and mix (M) with the correspondent iron addition treatments (S+ and M+). Different symbols denote treatments and timepoints that were found to be significantly different ($p < 0.05$) within the same experiment and same region (each panel).

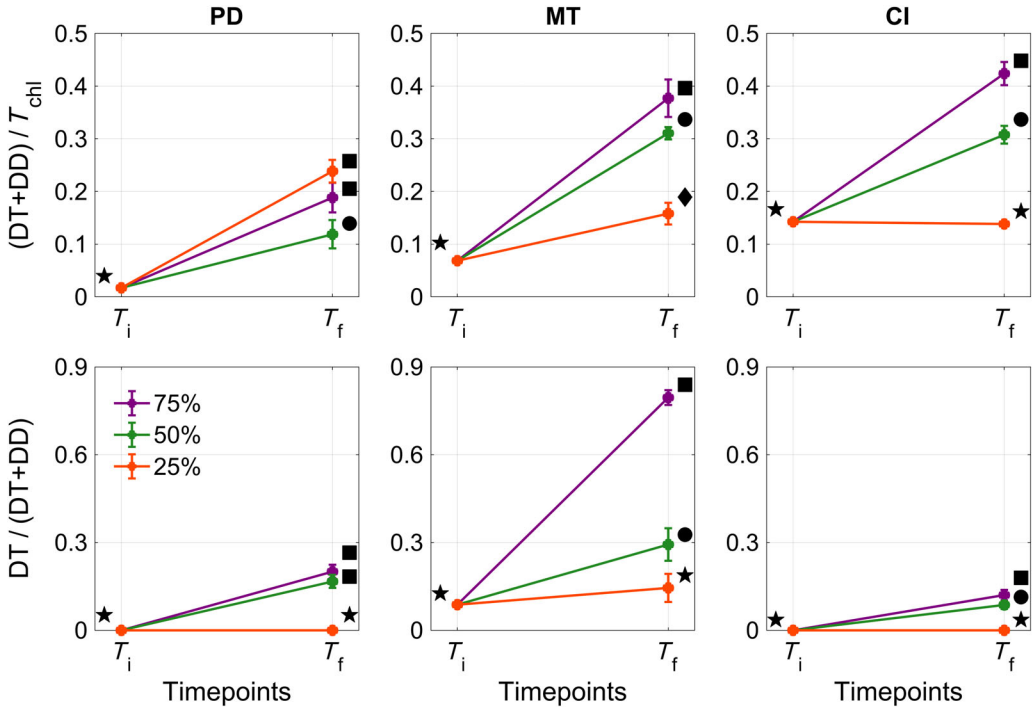

Fig. 6. Pigment ratios indicative of photoprotective strategies for the light treatments. Ratios involve diatoxathin (DT), diadinoxanthin (DD), and/or total chlorophyll (T_{chl}), at initial setup (T_i) and after 4 d (T_f) for PD (left), MT (middle), and canyon near CI (right). Light treatments are shown as the percentage of surface irradiance (75%, 50%, and 25%). Different symbols denote treatments and timepoints that were found to be significantly different ($p < 0.05$) for the same ratio and same region (each panel).

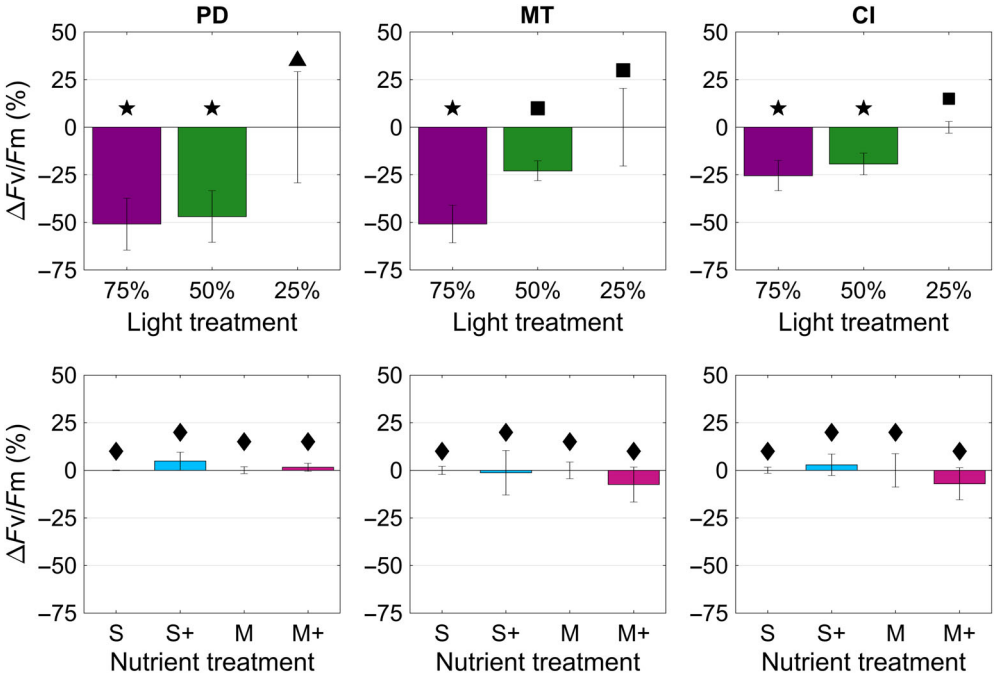

Fig. 7. Relative change (%) and standard deviation in photosynthetic efficiency ($\Delta F_v/F_m$) at T_f for PD (left), MT (middle), and canyon near CI (right) compared to T_f of the control treatment. Results shown for (top) light experiments, with treatments as percentage of surface irradiance (75%, 50%, and 25%) and where control is the lowest irradiance; (bottom) for nutrient experiments, where controls are shown as surface (S) and mix (M) with the corresponding iron addition treatments (S+ and M+). Different symbols denote treatments and timepoints that were found to be significantly different ($p < 0.05$) within the same experiment and same region (each panel).

irradiance levels. Compared to the lowest (control) irradiance, the 75% irradiance yielded a reduction of 50% in F_v/F_m.

No significant differences were found for the nutrient addition treatments, although a decrease in photosynthetic efficiency was found, likely due to the relatively high light (50% screening) to which the bottles were exposed. Chlorophyll increases were found in all nutrient treatments, although neither the added "deep" water (M treatment) nor the iron addition treatments ("+") showed different growth compared to the surface (S) control treatment. This growth at MT is thus consistent with a photoacclimation response to higher light than to any nutrient addition, further suggesting the lack of nutrient limitation at MT. Ratios of conversion of DD to DT are consistent with this photoacclimation response, with the highest irradiance tested showing increased response. The high production of photoprotective pigments can potentially explain why total chlorophyll was statistically unchanged ($p > 0.05$).

Canyon near CI

The region near CI showed the shallowest MLD, likely the result from extensive sea ice melting in the region, as evident from the low salinity at the surface (Fig. 1c, gold line). Community composition was more diverse than at the two other sites, with diatoms composing half the phytoplankton community and haptophytes and mixed flagellates the other half (Fig. 4). Cryptophytes were present but at low concentrations. Despite low phytoplankton concentrations in the source waters (0.25 μg L^{-1} initial Chl *a*), likely a consequence of more persistent sea ice cover all year round at that location (Kavanaugh et al. 2015), significant growth ($p < 0.05$) was seen in all treatments at the end of the incubation experiments, with highest irradiance (75%) yielding the lowest total Chl *a*. The T_{chl} results were statistically similar between the two lowest irradiances (25% and 50%) and the nutrient enrichment treatments, showing once again that phytoplankton were not nutrient-limited and were instead controlled by solar irradiance.

Based on the PAR profile (Fig. 3c) and the recorded responses to varying irradiance treatments, phytoplankton populations at CI were acclimated to higher light conditions than were present at the other regions; the 1% light level (47.5 m) at CI was well below the MLD (15 m). This, to large degree, explains the lower phytoplankton biomass in this location. No long-term increase in the photoprotective pigment pool ($[DT + DD]/T_{chl}$, (Fig. 6) was recorded for the lowest irradiance tested, showing that the ML-averaged light level (Fig. 3a; Table 2) to which phytoplankton were acclimated was higher than the 25% irradiance tested (106 μmol m^{-2} s^{-1}), consistent with our estimated MLD_{ave} light level (198 μmol m^{-2} s^{-1}).

Contrary to the other two regions, CI showed increases in photosynthetic efficiency in all light treatments (Table 3), ranging from 22% to 64%, suggesting phytoplankton were able to photoacclimate easily within the timescale of the incubation experiment, even at the highest irradiance. Despite increasing relative to the initial timepoint (Table 3), F_v/F_m for

the highest light treatment (75%) at T_4 was significantly lower than the lowest irradiance tested for the same timepoint (Fig. 7). For the nutrient additions, CI showed significant increases in T_{chl} on all treatments, but all treatments responded similarly, showing that iron addition did not yield significant increases in chlorophyll.

Discussion

Major penguin breeding colonies around Anvers, Avian, and Charcot Islands are associated with cross-shelf submarine canyon systems where increased chlorophyll has been recorded throughout the spring/summer season (Prézelin et al. 2000; Ducklow et al. 2012; Oliver et al. 2013; Kavanaugh et al. 2015; Kim et al. 2018). These canyons act as conduits for warm, nutrient-enriched deep mUCDW to penetrate to the nearshore regions (Prézelin et al. 2004; Martinson et al. 2008). Relatively high sea surface temperatures resulting from the intrusion of mUCDW have been hypothesized to result in earlier sea ice retreat, increased melting, shallower MLD, and increased chlorophyll (Kavanaugh et al. 2015). The hypothesis that recurrent pulses of mUCDW replenish surface waters with abundant macro- and micronutrients required to fuel primary production (Prézelin et al. 2000, 2004) is plausible, yet the results from this and other recent studies (Carvalho et al. 2016; Annett et al. 2017; Bown et al. 2017; Sherrell et al. 2018) do not support this hypothesis. Our analysis reveals that neither mixing deep water with surface water (simulating upwelling of mUCDW) nor iron enrichment stimulated phytoplankton growth, as nutrients were already abundant in the nearshore surface layers. While we recognize that only one set of experiments were reported at each location, comparison of the physical and biogeochemical dynamics at these timepoints and locations with the 25-yr time series collected for the PAL-LTER project in the WAP, show that the physical setting observed this year was not statistically different from the previous ones (Supporting Information Fig. S1). Also, high-resolution autonomous underwater glider-based surveys at the head of PD showed that although intrusion and mixing of mUCDW to the euphotic zone does occur near Anvers Island (Carvalho et al. 2016), the timing of these events is important, as winter water is present throughout the duration of the spring and summer phytoplankton blooms. Though this water mass was eroded slowly both from above and below, it acted as a physical barrier preventing the warm, deep (and nutrient enriched) water from mixing with surface waters during the bloom season. A recent study at PD has shown that local supply of iron to the upper ocean in the canyon is derived primarily from shallow sediment resuspension (Sherrell et al. 2018), further supporting the notion that mUCDW does not play a key role in nutrient input throughout the growth season. Additionally, the lack of a response to micronutrient additions in all of the treatments suggests that surface waters were indeed iron-replete.

So, why are WAP biological hotspots linked to the presence of canyons? While it is clear that the canyon regions foster unique surface circulation that concentrate phytoplankton (Kohut et al. 2018), we can also assert that the presence of canyons facilitates the reduction of the sea ice concentration earlier in the season through the upwelling of warm waters, promoting the light penetration into the water column in ice-free zones, especially in the Southern WAP where ice is still consistently present throughout the winter season (Kavanaugh et al. 2015). The increased sea ice melting in canyon regions leads to shallower MLD and increased stratification, both linked to increased phytoplankton concentrations (Mitchell and Holm-Hansen 1991; Moline and Prezelin 1996; Carvalho et al. 2016). A shallow MLD and enhanced water column stratification resulting from freshwater input from glacial and sea ice melt (Meredith et al. 2008; Schofield et al. 2018), low wind speeds over weekly timescales (Moline and Prezelin 1996; Moline 1998), and surface warming from incoming solar radiation provide a more favorable light environment for phytoplankton to thrive. This is beneficial in regions with persistent winter sea ice (Southern region), where the clearing of the ice opens up regions that phytoplankton can access with sufficient light to thrive (Montes-Hugo et al. 2009). However, in the Northern region (Palmer Deep), earlier ice retreat has little to no benefit for primary production because the ice-free season represents a longer proportion of the year (Stammerjohn et al. 2008). Warmer temperatures and decreased salinities can cause earlier shifts in the phytoplankton population from diatoms to cryptophytes (Moline et al. 2004; Rozema et al. 2017; Schofield et al. 2017), with repercussions for the food web (Schofield et al. 2010). Open water over longer periods of time together with increased winds can result in deeper MLD (Venables et al. 2013), which will limit primary production even if Fe is replete. The deepening of the ML can also replenish iron (Sherrell et al. 2018) through upward mixing of iron throughout the summer season. This is consistent with the observation at PD that while iron does decrease in the upper ocean as phytoplankton biomass increases, it does not become limiting (Carvalho et al. 2016). Warmer surface waters and less persistent sea ice will result in a less pronounced (both thickness and absolute temperature) winter water layer, which influences water column stratification (Venables et al. 2013; Carvalho et al. 2016). Increased winds deepen the ML, resulting in further decreases in primary production.

The latitudinal patterns of primary productivity and phytoplankton community composition along the WAP are heavily associated with geographic differences. These differences reflect the latitudinal differences in the timing of the sea ice retreat along with changing wind patterns and incident solar radiation at the surface (Montes-Hugo et al. 2009). Phytoplankton communities dominated by diatoms and cryptophytes have been previously reported for the Northernmost sites in the WAP (Montes-Hugo et al. 2009; Schofield et al. 2017). Long-term records in the Northern regions of the WAP have shown a

transition in the past three decades from diatom-dominated communities (Garibotti et al. 2003*a*) to smaller-celled phytoplankton assemblages such as cryptophytes (Moline and Prezelin 1996; Moline et al. 2004; Montes-Hugo et al. 2009). Our observations at Palmer Deep support these results, with this northern canyon showing a codominance of diatoms and cryptophytes. MT, the canyon in the middle of the peninsula, was completely dominated by diatoms, a result consistent with the productivity time series collected at the nearby United Kingdom Rothera Research Station (Rozema et al. 2017). Using satellite ocean color, the same observations were made, where higher Chl *a* and fucoxanthin, a diatom characteristic pigment, were detected at this middle site, compared to the other canyon systems in the WAP (Kavanaugh et al. 2015). Highest T_{chl} was observed at MT, where shallow ML, more stratified water columns and ample supply of nutrients result in increased biomass. If, over decadal time periods, there is a continued expansion of the wet and warm subpolar climate, it is hypothesized that MT will soon resemble the conditions seen now at PD. While studies of phytoplankton dynamics in the region around CI are scarce mainly because the canyon has not been accessible by ship until recently, it is thought that the dynamics seen in the MT region are still representative of the southernmost region (Montes-Hugo et al. 2009; Kavanaugh et al. 2015). If the wet and warm subpolar environment continues to migrate southward with current warming, CI will likely show increased production (similarly to MT; Montes-Hugo et al. 2009) as a wider area will be ice-free for longer periods of the summer season, creating a more favorable light environment for local primary production.

Phytoplankton are exposed to continuous variations in light due to changes in cloud cover and vertical mixing within the water column (Sakshaug and Slagstad 1991). Both the depth of the ML and the rate of mixing are crucial in controlling the light available to the phytoplankton (Mitchell and Holm-Hansen 1991). Phytoplankton respond to these variations in the light field by photoadaptive mechanisms (Sakshaug and Holm-Hansen 1986) that tend to optimize photosynthetic rates and growth under light-limiting conditions. Photosynthetic efficiency of Photosystem II (F_v/F_m) for the initial population was lower (0.4) than maximum values (0.55–0.65) typically observed in nutrient-replete cultures of phytoplankton (Kolber et al. 1988) and in nutrient-replete phytoplankton communities in the Southern ocean (Gervais et al. 2002; Coale et al. 2004), but it was markedly higher than F_v/F_m observed in Fe-limited regions (≤ 0.2, Gervais et al. 2002; Coale et al. 2004; Park et al. 2017), indicating that phytoplankton in the source water were possibly already under some environmental stress. Source water was collected from the surface, so intermediate values of F_v/F_m may be an indication that phytoplankton were exposed to higher light than that to which they were originally adapted. Also, changes in community composition are known to affect the photosynthetic efficiency of a phytoplankton population (Suggett et al. 2009), but data are not available to evaluate these effects in this incubation.

Under high-light conditions, phytoplankton are able to prevent photo-oxidative damage by investing in the production of photoprotective pigments, as evident from an increase in the ratio of photoprotective pigments to chlorophyll ($[DT + DD]/T_{chl}$). Our light experiments have shown that in a stable and moderate light environment (e.g., in a shallow MLD), phytoplankton are able to acclimate to light on the timescale of a few days (Schofield et al. 1995), consistent with previous work linking increased chlorophyll to a stable and shallow MLD (Moline and Prezelin 1996; Venables et al. 2013; Carvalho et al. 2016). Differences in the photoacclimation response at Palmer Deep compared to the Southern canyons, where the 50% light treatment showed chlorophyll increases despite the initial lower light acclimation, could be explained by the dominance of diatoms in the Southern regions, as diatoms are better suited for adapting to higher irradiance levels (Arrigo et al. 2010; Mills et al. 2010).

In summary, this study supports the hypothesis that light, not nutrient intrusions from mUCDW, control phytoplankton biomass and physiology in biological hotspots along the WAP. While all of the light exposures tested (75%, 50%, and 25% of incident radiation) were higher than in situ light levels sampled, phytoplankton were able to rapidly photoacclimate to the incubation light level. Results from the nutrient enrichment incubation experiments do not support the Canyon Hypothesis (Schofield et al. 2013) that postulates that the nutrient enrichment (Prézelin et al. 2000, 2004) from the upwelling of warm, deep mUCDW is responsible for the increased phytoplankton biomass observed at these locations. This is consistent with observations that suggest macro- and micronutrients in surface waters at these locations are replete (Sherrell et al. 2018). The three locations show very different ice conditions (Stammerjohn et al. 2008; Kavanaugh et al. 2015), setting up different MLD dynamics that in turn affect the phytoplankton community response to light. Our results are also consistent with previous studies of the temporal evolution of the water masses at the canyon head at Palmer Deep (Carvalho et al. 2016) where, although there is evidence of an upward intrusion of mUCDW at the northernmost site, this water mass does not reach the upper 100 m until after the spring bloom ends. The uplift of this water mass can, however, potentially influence the depth of the winter water layer which sets up the water column stratification, the depth of the ML, and the nutrient pool available to the following year's bloom. Given changing MLDs associated with declining ice (Schofield et al. 2018), the overall productivity and ecosystem dynamics will be affected. The north-south gradient of declining sea ice will move southward, likely resulting in further decreases in phytoplankton and/or changes in community composition. Phytoplankton light adaptations to dynamic environments will then be key to their success, and to the consequent carbon export.

References

Annett, A. L., and others. 2015. Comparative roles of upwelling and glacial iron sources in Ryder Bay, coastal western Antarctic Peninsula. Mar. Chem. **176**: 21–33. doi:10.1016/j.marchem.2015.06.017

Annett, A. L., and others. 2017. Controls on dissolved and particulate iron distributions in surface waters of the Western Antarctic Peninsula shelf. Mar. Chem. **196**: 81–97. doi:10.1016/j.marchem.2017.06.004

Arrigo, K. R., M. M. Mills, L. R. Kropuenske, G. L. van Dijken, A.-C. Alderkamp, and D. H. Robinson. 2010. Photophysiology in two major Southern Ocean phytoplankton taxa: Photosynthesis and growth of *Phaeocystis antarctica* and *Fragilariopsis cylindrus* under different irradiance levels. Integr. Comp. Biol. **50**: 950–966. doi:10.1093/icb/icq021

Bernard, K. S., D. K. Steinberg, and O. M. Schofield. 2012. Summertime grazing impact of the dominant macrozooplankton off the Western Antarctic Peninsula. Deep-Sea Res. Part I Oceanogr. Res. Pap. **62**: 111–122. doi:10.1016/j.dsr.2011.12.015

Bown, J., P. Laan, S. Ossebaar, K. Bakker, P. Rozema, and H. J. W. de Baar. 2017. Bioactive trace metal time series during Austral summer in Ryder Bay, Western Antarctic Peninsula. Deep-Sea Res. Part II Top. Stud. Oceanogr. **139**: 103–119. doi:10.1016/j.dsr2.2016.07.004

Brunet, C., J. M. Brylinski, and Y. Lemoine. 1993. In-situ variations of the xanthophylls diatoxanthin and diadinoxanthin - photoadaptation and relationships with a hydrodynamical system in the eastern English-Channel. Mar. Ecol. Prog. Ser. **102**: 69–77. doi:10.3354/meps102069

Carvalho, F., J. Kohut, M. J. Oliver, R. M. Sherrell, and O. Schofield. 2016. Mixing and phytoplankton dynamics in a submarine canyon in the West Antarctic Peninsula. J. Geophys. Res. Oceans **121**: 5069–5083. doi:10.1002/2016JC011650

Carvalho, F., J. Kohut, M. J. Oliver, and O. Schofield. 2017. Defining the ecologically relevant mixed-layer depth for Antarctica's coastal seas. Geophys. Res. Lett. **44**: 338–345. doi:10.1002/2016GL071205

Clarke, A., M. P. Meredith, M. I. Wallace, M. A. Brandon, and D. N. Thomas. 2008. Seasonal and interannual variability in temperature, chlorophyll and macronutrients in northern Marguerite Bay, Antarctica. Deep-Sea Res. Part II Top. Stud. Oceanogr. **55**: 1988–2006. doi:10.1016/j.dsr2.2008.04.035

Coale, K. H., and others. 2004. Southern Ocean iron enrichment experiment: Carbon cycling in high- and low-Si waters. Science **304**: 408–414. doi:10.1126/science.1089778

Couto, N., D. G. Martinson, J. Kohut, and O. Schofield. 2017. Distribution of upper circumpolar deep water on the warming continental shelf of the West Antarctic Peninsula. J. Geophys. Res. Oceans **122**: 5306–5315. doi:10.1002/2017JC012840

Cullen, J. J., and M. R. Lewis. 1988. The kinetics of algal photoadaptation in the context of vertical mixing. J. Plankton Res. **10**: 1039–1063. doi:10.1093/plankt/10.5.1039

de Baar, H. J. W., and others. 2005. Synthesis of iron fertilization experiments: From the iron age in the age of enlightenment. J. Geophys. Res. Oceans **110**: C09S16. doi:10.1029/2004JC002601

Demers, S., S. Roy, R. Gagnon, and C. Vignault. 1991. Rapid light-induced changes in cell fluorescence and in xantophyll-cycle pigments of *Alexandrium excavatum* (Dinophyceae) and *Thalasiosira pseudonana* (Bacillariophyceae): A photoprotection mechanism. Mar. Ecol. Prog. Ser. **76**: 185–193. doi:10.3354/meps076185

Ducklow, H., and others. 2012. The Marine System of the Western Antarctic Peninsula. *In* A. D. Rogers, N. M. Johnston, E. J. Murphy and A. Clarke [Eds.], Antarctic Ecosystems. doi:10.1002/9781444347241.ch5

Erdmann, E. S., C. A. Ribic, D. L. Patterson-Fraser, and W. R. Fraser. 2011. Characterization of winter foraging locations of Adelie penguins along the Western Antarctic Peninsula, 2001-2002. Deep-Sea Res. Part II Top. Stud. Oceanogr. **58**: 1710–1718. doi:10.1016/j.dsr2.2010.10.054

Falkowski, P. G., and J. Raven. 2007. Aquatic photosynthesis. Princeton Univ. Press. ISBN 9780691115511.

Fraser, W. R., and W. Z. Trivelpiece. 1996. Factors controlling the distribution of seabirds: Winter-summer heterogeneity in the distribution of Adélie penguin populations. Antarct. Res. Ser. **70**: 257–272. doi:10.1029/AR070p0257

Fujiki, T., T. Toda, T. Kikuchi, and S. Taguchi. 2003. Photoprotective response of xanthophyll pigments during phytoplankton blooms in Sagami Bay, Japan. J. Plankton Res. **25**: 317–322. doi:10.1093/plankt/25.3.317

Garibotti, I. A., M. Vernet, M. E. Ferrario, R. C. Smith, R. M. Ross, and L. B. Quetin. 2003*a*. Phytoplankton spatial distribution patterns along the western Antarctic Peninsula (Southern Ocean). Mar. Ecol. Prog. Ser. **261**: 21–39. doi:10.3354/meps261021

Garibotti, I., M. Vernet, W. A. Kozlowski, and M. E. Ferrario. 2003*b*. Composition and biomass of phytoplankton assemblages in coastal Antarctic waters: A comparison of chemotaxonomic and microscopic analyses. Mar. Ecol. Prog. Ser. **247**: 27–42. doi:10.3354/meps247027

Garibotti, I. A., M. Vernet, R. C. Smith, and M. E. Ferrario. 2005. Interannual variability in the distribution of the phytoplankton standing stock across the seasonal sea-ice zone west of the Antarctic Peninsula. J. Plankton Res. **27**: 825–843. doi:10.1093/plankt/fbi056

Gervais, F., U. Riebesell, and M. Y. Gorbunov. 2002. Changes in primary productivity and chlorophyll a in response to iron fertilization in the Southern Polar Frontal Zone. Limnol. Oceanogr. **47**: 1324–1335. doi:10.4319/lo.2002.47.5.1324

Gorbunov, M. Y., and P. G. Falkowski. 2004. Fluorescence induction and relaxation (FIRe) technique and instrumentation for monitoring photosynthetic processes and primary production in aquatic ecosystems, p. 1029–1031. *In* A. van der Est & D. Bruce (Eds.), Photosynthesis: Fundamental

aspects to global perspectives—Proc. 13th International Congress of Photosynthesis, Allen Press, Montreal, August.

Holm-Hansen, O., and B. Mitchell. 1991. Spatial and temporal distribution of phytoplankton and primary production in the western Bransfield Strait region. Deep-Sea Res. Part I Oceanogr. Res. Pap. **38**: 961–980. doi:10.1016/0198-0149(91)90092-T

Hopkinson, B. M., and others. 2007. Iron limitation across chlorophyll gradients in the southern Drake Passage: Phytoplankton responses to iron addition and photosynthetic indicators of iron stress. Limnol. Oceanogr. **52**: 2540–2554. doi:10.4319/lo.2007.52.6.2540

Kavanaugh, M. T., and others. 2015. Effect of continental shelf canyons on phytoplankton biomass and community composition along the western Antarctic Peninsula. Mar. Ecol. Prog. Ser. **524**: 11–26. doi:10.3354/meps11189

Kim, H., S. C. Doney, R. A. Iannuzzi, M. P. Meredith, D. G. Martinson, and H. W. Ducklow. 2016. Climate forcing for dynamics of dissolved inorganic nutrients at Palmer Station, Antarctica: An interdecadal (1993–2013) analysis. J. Geophys. Res. Biogeosci. **121**: 2369–2389. doi:10.1002/2015JG003311

Kim, H., and others. 2018. Inter-decadal variability of phytoplankton biomass along the coastal West Antarctic Peninsula. Philos. Trans. R. Soc. A Math. Phys. Eng. Sci. **376**: 1–21. doi:10.1098/rsta.2017.0174

Kohut, J. T., and others. 2018. Variability in summer surface residence time within a West Antarctic Peninsula biological hotspot. Philos. Trans. R. Soc. A Math. Phys. Eng. Sci. **376**: 20170165. doi:10.1098/rsta.2017.0165

Kolber, Z., J. Zehr, and P. Falkowski. 1988. Effects of growth irradiance and nitrogen limitation on photosynthetic energy conversion in photosystem II. Plant Physiol. **88**: 923–929. doi:10.1104/pp.88.3.923

Kozlowski, W. A., D. Deutschman, I. Garibotti, C. Trees, and M. Vernet. 2011. An evaluation of the application of CHEMTAX to Antarctic coastal pigment data. Deep-Sea Res. Part I Oceanogr. Res. Pap. **58**: 350–364. doi:10.1016/j.dsr.2011.01.008

Lagerström, M., M. Field, M. Séguret, L. Fischer, S. Hann, and R. Sherrell. 2013. Automated on-line flow-injection ICP-MS determination of trace metals (Mn, Fe, Co, Ni, Cu and Zn) in open ocean seawater: Application to the GEOTRACES program. Mar. Chem. **155**: 71–80. doi:10.1016/j.marchem.2013.06.001

Lewis, M. R., J. J. Cullen, and T. Platt. 1984. Relationships between vertical mixing and photoadaptation of phytoplankton - similarity criteria. Mar. Ecol. Prog. Ser. **15**: 141–149. doi:10.3354/meps015141

Mackey, M. D., D. J. Mackey, H. W. Higgins, and S. W. Wright. 1996. CHEMTAX - a program for estimating class abundances from chemical markers: Application to HPLC measurements of phytoplankton. Mar. Ecol. Prog. Ser. **144**: 265–283. doi:10.3354/meps144265

Martinson, D. G., S. E. Stammerjohn, R. A. Iannuzzi, R. Smith, and M. Vernet. 2008. Western Antarctic Peninsula physical oceanography and spatio-temporal variability. Deep-Sea Res. Part II Top. Stud. Oceanogr. **55**: 1964–1987. doi:10.1016/j.dsr2.2008.04.038

Martinson, D. G., and D. C. McKee. 2012. Transport of warm upper circumpolar deep water onto the Western Antarctic Peninsula continental shelf. Ocean Sci. **8**: 433–442. doi:10.5194/os-8-433-2012

McKee, D. C., D. G. Martinson, and O. Schofield. 2019. Origin and attenuation of mesoscale structure in circumpolar deep water intrusions to an Antarctic shelf. J. Phys. Oceanogr. **49**: 1293–1318. doi:10.1175/JPO-D-18-0133.1

Meredith, M. P., and others. 2008. Variability in the freshwater balance of northern Marguerite Bay, Antarctic Peninsula: Results from $\delta^{18}O$. Deep-Sea Res. Part II Top. Stud. Oceanogr. **55**: 309–322. doi:10.1016/j.dsr2.2007.11.005

Mills, M. M., and others. 2010. Photophysiology in two Southern Ocean phytoplankton taxa: Photosynthesis of *Phaeocystis Antarctica* (Prymnesiophyceae) and *Fragilariopsis cylindrus* (Bacillariophyceae) under simulated mixed-layer irradiance. J. Phycol. **46**: 1114–1127. doi:10.1111/j.1529-8817.2010.00923.x

Mitchell, B. G., and O. Holm-Hansen. 1991. Observations of modeling of the Antarctic phytoplankton crop in relation to mixing depth. Deep-Sea Res. Part I Oceanogr. Res. Pap. **38**: 981–1007. doi:10.1016/0198-0149(91)90093-U

Mobley, C. D. 1994. Light and water: Radiative transfer in natural waters. Academic Press. ISBN 0125027508, 9780125027502.

Moline, M. 1998. Photoadaptive response during the development of a coastal Antarctic diatom bloom and relationship to water column stability. Limnol. Oceanogr. **43**: 146–153. doi:10.4319/lo.1998.43.1.0146

Moline, M., and B. B. Prezelin. 1996. Long-term monitoring and analyses of physical factors regulating variability in coastal Antarctic phytoplankton biomass, in situ productivity and taxonomic composition over subseasonal, seasonal and interannual time scales. Mar. Ecol. Prog. Ser. **145**: 143–160. doi:10.3354/meps145143

Moline, M., H. Claustre, T. K. Frazer, O. Schofield, and M. Vernet. 2004. Alteration of the food web along the Antarctic Peninsula in response to a regional warming trend. Glob. Chang. Biol. **10**: 1973–1980. doi:10.1111/j.1365-2486.2004.00825.x

Montes-Hugo, M. A., and others. 2009. Recent changes in phytoplankton communities associated with rapid regional climate change along the Western Antarctic Peninsula. Science **323**: 1470–1473. doi:10.1126/science.1164533

Nelson, D. M., and W. Smith. 1991. The role of light and major nutrients. Limnol. Oceanogr. **36**: 1650–1661. doi:10.4319/lo.1991.36.8.1650

Oliver, M. J., and others. 2013. Adelie penguin foraging location predicted by tidal regime switching. PLoS One **e55163**: 8. doi:10.1371/journal.pone.0055163

Park, J., and others. 2017. Light availability rather than Fe controls the magnitude of massive phytoplankton bloom

in the Amundsen Sea polynyas, Antarctica. Limnol. Oceanogr. **62**: 2260–2276. doi:10.1002/lno.10565

Prézelin, B. B., E. E. Hofmann, C. Mengelt, and J. M. Klinck. 2000. The linkage between Upper Circumpolar Deep Water (UCDW) and phytoplankton assemblages on the West Antarctic Peninsula continental shelf. J. Mar. Res. **58**: 165–202. doi:10.1357/002224000321511133

Prézelin, B. B., E. E. Hofmann, M. Moline, and J. M. Klinck. 2004. Physical forcing of phytoplankton community structure and primary production in continental shelf waters of the Western Antarctic Peninsula. J. Mar. Res. **62**: 419–460. doi:10.1357/0022240041446173

Rozema, P. D., H. J. Venables, W. H. van de Poll, A. Clarke, M. P. Meredith, and A. G. J. Buma. 2017. Interannual variability in phytoplankton biomass and species composition in northern Marguerite Bay (West Antarctic Peninsula) is governed by both winter sea ice cover and summer stratification. Limnol. Oceanogr. **62**: 235–252. doi:10.1002/lno.10391

Saba, G. K., and others. 2014. Winter and spring controls on the summer food web of the coastal West Antarctic Peninsula. Nat. Commun. **5**: 4318. doi:10.1038/ncomms5318

Sakshaug, E., and O. Holm-Hansen. 1986. Photoadaptation in Antarctic phytopfankton: Variations in growth rate, chemical composition and P versus I curves. J. Plankton Res. **8**: 459–473. doi:10.1093/plankt/8.3.459

Sakshaug, E., G. Johnsen, K. Andresen, and M. Vernet. 1991. Modeling of light-dependent algal photosynthesis and growth: Experiments with the Barents Sea diatoms *Thalassiosira nordenskioldii* and *Chaetoceros furcellatus*. Deep-Sea Res. Part I Oceanogr. Res. Pap. **38**: 415–430. doi:10.1016/0198-0149(91)90044-G

Sakshaug, E., and D. Slagstad. 1991. Light and productivity of phytoplankton in polar marine ecosystems: A physiological view. Polar Res. **10**: 69–86. doi:10.1111/j.1751-8369.1991.tb00636.x

Schofield, O., M. A. Moline, and B. B. Prezelin. 1995. Palmer LTER: Photoacclimation in a coastal phytoplankton bloom. Antarct J US. **30**: 260–262.

Schofield, O., H. W. Ducklow, D. G. Martinson, M. P. Meredith, M. A. Moline, and W. R. Fraser. 2010. How do polar marine ecosystems respond to rapid climate change? Science **328**: 1520–1523. doi:10.1126/science.1185779

Schofield, O., and others. 2013. Penguin biogeography along the West Antarctic Peninsula: Testing the canyon hypothesis with Palmer LTER observations. Oceanography **26**: 204–206. doi:10.5670/oceanog.2013.63

Schofield, O., and others. 2017. Decadal variability in coastal phytoplankton community composition in a changing West Antarctic Peninsula. Deep-Sea Res. Part I Oceanogr. Res. Pap. **124**: 42–54. doi:10.1016/j.dsr.2017.04.014

Schofield, O., and others. 2018. Changes in the upper ocean mixed layer and phytoplankton productivity along the West Antarctic Peninsula. Philos. Trans. R. Soc. A Math. Phys. Eng. Sci. **376**: 20170173. doi:10.1098/rsta.2017.0173

Serebrennikova, Y. M., and K. A. Fanning. 2004. Nutrients in the Southern Ocean GLOBEC region: Variations, water circulation, and cycling. Deep-Sea Res. Part II Top. Stud. Oceanogr. **51**: 1981–2002. doi:10.1016/j.dsr2.2004.07.023

Sherrell, R. M., A. L. Annett, J. N. Fitzsimmons, V. J. Roccanova, and M. P. Meredith. 2018. A 'shallow bathtub ring' of local sedimentary iron input maintains the Palmer Deep biological hotspot on the West Antarctic Peninsula shelf. Philos. Trans. R. Soc. A Math. Phys. Eng. Sci. **376**: 20170171. doi:10.1098/rsta.2017.0171

Smith, R., D. G. Martinson, S. E. Stammerjohn, R. A. Iannuzzi, and K. Ireson. 2008. Bellingshausen and western Antarctic Peninsula region: Pigment biomass and sea-ice spatial/temporal distributions and interannual variabilty. Deep-Sea Res. Part II Top. Stud. Oceanogr. **55**: 1949–1963. doi:10.1016/j.dsr2.2008.04.027

Stammerjohn, S. E., D. G. Martinson, R. C. Smith, and R. A. Iannuzzi. 2008. Sea ice in the western Antarctic Peninsula region: Spatio-temporal variability from ecological and climate change perspectives. Deep-Sea Res. Part II Top. Stud. Oceanogr. **55**: 2041–2058. doi:10.1016/j.dsr2.2008.04.026

Suggett, D. J., C. M. Moore, A. E. Hickman, and R. J. Geider. 2009. Interpretation of fast repetition rate (FRR) fluorescence: signatures of phytoplankton community structure versus physiological state. Mar Ecol Prog Ser. **376**: 1–19. doi:10.3354/meps07830

Venables, H. J., A. Clarke, and M. P. Meredith. 2013. Wintertime controls on summer stratification and productivity at the western Antarctic Peninsula. Limnol. Oceanogr. **58**: 1035–1047. doi:10.4319/lo.2013.58.3.1035

Wright, S. 1991. Improved HPLC method for the analysis of chlorophylls and carotenoids from marine phytoplankton. Mar. Ecol. Prog. Ser. **77**: 183–196. doi:10.3354/meps077183

Acknowledgments

We thank Mansha Pasticha and Cheryl Zubrick for help with incubation setups; Lora McGuinness, Naomi Shelton, and Joe Roccanova for help analyzing HPLC pigments, nutrients, and trace metal concentrations. We also thank the crew and support staff of ARSV *Laurence M. Gould* during LMG15-01. This research was supported by the National Science Foundation grant ANT-0823101 (Palmer-LTER). Filipa Carvalho was funded by a Portuguese doctoral fellowship from Fundação para a Ciência e Tecnologia (DFRH - SFRH/BD/72705/2010), a Teledyne Marine Graduate Fellowship, and a European Research Council Consolidator grant (GOCART, agreement 724416).

Conflict of Interest

None declared.

Submitted 02 September 2018
Revised 27 June 2019
Accepted 31 July 2019

Associate editor: Anya Waite